Spectrum inference for replicated spatial locally time-harmonizable time series

John Aston, Dominique Dehay, Anna E. Dudek, Jean-Marc Freyermuth, Denes Szucs, Lincoln Colling

Spectrum inference for replicated spatial locally time-harmonizable time series

John Aston
Dept. of Pure Mathematics and Mathematical Statistics,
University of Cambridge, U.K.
and
Dominique Dehay
University of Rennes, CNRS, IRMAR UMR 6625, France
and
Anna E. Dudek
AGH University of Science and Technology, Dept. of Applied Mathematics, Poland *
and
Jean-Marc Freyermuth
Institut de Mathématiques de Marseille, Aix-Marseille University, France.
and
Denes Szucs
Dept. of Psychology, University of Cambridge, U.K.†
and
Lincoln Colling
Dept. of Psychology, University of Sussex, U.K.

March 6, 2022

Abstract

In this paper we develop tools for statistical inference on replicated realizations of spatiotemporal processes that are locally time-harmonizable. Our method estimates both the rescaled spatial time-varying Loève-spectrum and the spatial time-varying

*Anna Dudek acknowledges support from the King Abdullah University of Science and Technology (KAUST) Research Grant OSR-2019-CRG8-4057.2.

†Denes Szucs and Lincoln Colling are funded by James S. McDonnell Foundation 21st Century Science Initiative in Understanding Human Cognition (grant number 220020370; received by Denes Szucs).

dual-frequency coherence function under realistic modeling assumptions. We construct confidence intervals for these parameters of interest using the Circular Block Bootstrap method and prove its consistency. We illustrate the application of our methodology on a dataset arising from an experiment in neuropsychology. From EEG recordings, our method allows to study the dynamic functional connectivity within the brain associated to visual working memory performance.

Keywords: Harmonizable spatiotemporal processes, nonparametric spectral analysis, Circular Block Bootstrap, functional connectivity, ElectroEncephaloGraphy.

1 Introduction

The paper is concerned with a class of spatiotemporal processes that are locally time-harmonizable, that is, they possess a local two-dimensional spectrum. In order to introduce such a class of processes, we need first to recall some basic facts concerning second order harmonizable processes that are due to Loève [1948]. A centered P-variate discrete-time process $\{\boldsymbol{X}_t\} = \{\boldsymbol{X}_t,\ t \in \mathbb{Z}\}$ with the finite second order moments is called harmonizable if it admits a Cramér's representation of the following form:

$$\boldsymbol{X}_t = \int_{-\pi}^{\pi} e^{it\omega} d\boldsymbol{Z}\left(\omega\right), \tag{1}$$

where $\boldsymbol{X}_t = (X_{1,t}, \ldots, X_{P,t})'$ and the spectral process
$\{\boldsymbol{Z}(\omega)\} = \{\boldsymbol{Z}(\omega) = (Z_1(\omega), \ldots, Z_P(\omega))',\ \omega \in (-\pi, \pi]\}$ is a zero-mean stochastic process. Here and hereafter the symbol $(\cdot)'$ denotes the transpose of a vector.

The simplest example of processes admitting the representation (1) are stationary sequences. In that case the process $\{\boldsymbol{Z}(\omega)\}$ has orthogonal and cross-orthogonal increments (see e.g., Brockwell and Davis [1991]). However, for the class of harmonizable processes, $\{\boldsymbol{Z}(\omega)\}$ has correlated increments. They form a broad class of processes that includes many nonstationary ones, such as periodically correlated time series. A very important feature of harmonizable processes is that their covariance is a Fourier transform of a finite measure.

Harmonizable processes are particularly useful in modeling real-world data when the main interest is frequency domain analysis. They are widely applied for instance in signal theory, communications and mechanics (see e.g., Napolitano [2016], Gardner et al. [2006], Setoodeh and Haykin [2017], Serpedin et al. [2005]). Our approach was initially motivated by the analysis of ElectroEncephaloGraphy (EEG) data. However, it can be applied to other types of problems with possibly some minor modifications.

In recent years, numerous studies of brain signals have explored networks of functional connections to reveal subtle mechanisms of brain activity. Essentially, this involves measuring the relationships in the activity of different brain regions. The analysis is often performed using coherence, which is a frequency domain equivalent of correlation. More specifically, for a P-variate harmonizable process $\{\boldsymbol{X}_t\}$, its Loève spectrum $\boldsymbol{f} = \left(f_{pq}\right)_{1\leq p,q\leq P}$ is a $P \times P$-matrix defined as follows

$$\mathrm{Cov}(d\boldsymbol{Z}(\omega_1), d\boldsymbol{Z}(\omega_2)) = \boldsymbol{f}(\omega_1, \omega_2) d\omega_1 d\omega_2. \tag{2}$$

The dual-frequency coherence between a pair of processes $(\{X_{p,t}\}, \{X_{q,t}\})$ and a pair of frequencies (ω_1, ω_2) is given by:

$$\begin{aligned} \rho_{pq}(\omega_1, \omega_2) &:= \frac{\left|\mathrm{Cov}\left(dZ_p(\omega_1), dZ_q(\omega_2)\right)\right|^2}{\mathrm{Var}\left(dZ_p(\omega_1)\right)\mathrm{Var}\left(dZ_q(\omega_2)\right)} \\ &= \frac{\left|f_{pq}(\omega_1, \omega_2)\right|^2}{f_{pp}(\omega_1, \omega_1) f_{qq}(\omega_2, \omega_2)}. \end{aligned} \tag{3}$$

The dual-frequency coherence (3) allows to capture dependencies at two different frequencies. Soedjak [2002] developed inference tools for the Loève spectrum for such a model, but the Loève spectrum of the harmonizable process is constant in time and the model does not consider any spatial localization. Therefore, it cannot sufficiently capture the complexity of the brain mechanisms. Consequently, these results needed to be extended accordingly. This was achieved thanks to the recent and important contribution of Gorrostieta et al. [2019]. The authors follow the approach of Dahlhaus [2012] to introduce multivariate locally-harmonizable processes. They describe a windowed Fourier based estimation procedure for the time-varying dual-frequency coherence. They derive exact confidence intervals for testing if the coherence differs from zero under i.i.d. Gaussian assumptions, and also obtain asymptotic confidence intervals.

In this paper, we extend the existing results in several ways. First, we introduce new inference tools that take into account both time and space (i.e. spatial location). We define the rescaled spatiotemporal local Loève spectrum and the spatiotemporal coherence. In other words, we measure the time-evolving squared correlation coefficient at different frequencies between any pairs of spatial locations. Our approach uses spatial correlations to improve the estimation of these quantities by exploiting spatial location information in the spirit of the Ombao et al. [2008] method. Second, we consider more realistic modeling assumptions. Third, in order to construct confidence intervals for the spatiotemporal coherence, we adapt the Circular Block Bootstrap (CBB) method and show its consistency.

The paper is organized as follows. In Section 2 we introduce a spatial locally time-harmonizable process model along with an appropriate estimation procedure under realistic model assumptions. In Section 3 we discuss asymptotic properties of our estimators. Moreover, we show consistency of the CBB approach. In Section 4, we present the results in the Gaussian framework. Finally, in Section 5 we illustrate the application of our method on a real data set. All proofs can be found in the companion document [Aston et al., 2022].

2 Rescaled spatiotemporal spectrum estimation

In this section we generalize some of the ideas presented by Ombao et al. [2008] and Gorrostieta et al. [2019]. For the sake of clarity, we start by introducing the notion of spatial time-harmonizable process and the corresponding Loève spectrum. Next, we introduce the spatial time-varying local Loève spectrum for a general spatial process. Then, we describe our modeling assumptions, in particular the spatiotemporal rescaling. We construct a rescaled spectrum estimator that is based on replicated observations of the process, and give its asymptotic properties. Finally, we adapt the CBB method to construct bootstrap confidence intervals and we prove the bootstrap consistency.

2.1 Spatiotemporal Loève spectrum

Let $\left\{\boldsymbol{X}_t^{\underline{S}}\right\} = \left\{\boldsymbol{X}_t^{\underline{S}}, t \in \mathbb{Z}\right\} := \left\{X_{\underline{s},t}^{\underline{S}}, t \in \mathbb{Z}, \underline{s} \in \{1,\dots,S_1\} \times \{1,\dots,S_2\}\right\}$, $\underline{S} := (S_1, S_2) \in \mathbb{N}^{*2}$, be a family of spatial time-harmonizable processes, i.e.,

$$\boldsymbol{X}_t^{\underline{S}} = \int_{-\pi}^{\pi} e^{i\omega t} d\boldsymbol{Z}^{\underline{S}}(\omega),$$

such that $\mathrm{Cov}\left(d\boldsymbol{Z}^{\underline{S}}(\omega_1), d\boldsymbol{Z}^{\underline{S}}(\omega_2)\right) = \boldsymbol{f}^{\underline{S}}(\omega_1,\omega_2)\, d\omega_1 d\omega_2$, where $\boldsymbol{f}^{\underline{S}} = \left(f_{\underline{s}_1,\underline{s}_2}^{\underline{S}}\right)_{\underline{s}_1,\underline{s}_2 \in \{1,\dots,S_1\}\times\{1,\dots,S_2\}}$ is the Loève spectrum. Then

$$\boldsymbol{C}^{\underline{S}}(t_1,t_2) := \mathrm{Cov}\left(\boldsymbol{X}_{t_1}^{\underline{S}}, \boldsymbol{X}_{t_2}^{\underline{S}}\right) = \int_{-\pi}^{\pi}\int_{-\pi}^{\pi} \boldsymbol{f}^{\underline{S}}(\omega_1,\omega_2)\, e^{i(\omega_1 t_1 - \omega_2 t_2)} d\omega_1 d\omega_2.$$

Notice that $\boldsymbol{C}^{\underline{S}}(t_1,t_2)$ and $\boldsymbol{f}^{\underline{S}}(\omega_1,\omega_2)$ are $S_1 \times S_2 \times S_1 \times S_2$-matrices. Here and in the sequel $\mathbb{N}^* := \{1,2,\dots\}$.

A sufficient condition for time-harmonizability and the existence of a two-dimensional spectral density for the discrete-time spatial second order random processes $\left\{\boldsymbol{X}_t^{\underline{S}}\right\}$ is given by the following condition

$$\sum_{(t_1,t_2)\in\mathbb{Z}^2} \left|\boldsymbol{C}^{\underline{S}}(t_1,t_2)\right| < \infty,$$

where $\boldsymbol{C}^{\underline{S}}(t_1,t_2) = \mathrm{Cov}\left(\boldsymbol{X}^{\underline{S}}_{t_1}, \boldsymbol{X}^{\underline{S}}_{t_2}\right)$. Then the Loève spectrum is a continuous function and it coincides with

$$\boldsymbol{f}^{\underline{S}}(\omega_1,\omega_2) = \frac{1}{4\pi^2} \sum_{(t_1,t_2)\in\mathbb{Z}^2} \boldsymbol{C}^{\underline{S}}(t_1,t_2)\, e^{-i(\omega_1 t_1 - \omega_2 t_2)}.$$

Remark that the above definition does not include the stationary case as the Loève spectrum is two-dimensional while the spectrum of a stationary process is one-dimensional.

2.2 Localized Loève spectrum

For the purpose of our application the notion of harmonizable processes is not sufficient. Therefore, in this section, we generalize the previous considerations by introducing the notion of spectrum (2) for a spatial second order process $\{\boldsymbol{X}^{\underline{S}}_t\}$ that is not necessarily time-harmonizable. We also introduce its estimator.
We define the (spatiotemporal) localized Loève spectrum of the process $\{\boldsymbol{X}^{\underline{S}}_t\}$ as

$$\breve{\boldsymbol{f}}^{\underline{S}}_{t_1,t_2}(\omega_1,\omega_2) := \frac{1}{4\pi^2} \sum_{k_1=t_1-N}^{t_1+N-1} \sum_{k_2=t_2-N}^{t_2+N-1} \boldsymbol{C}^{\underline{S}}(k_1,k_2) e^{-i(\omega_1 k_1 - \omega_2 k_2)} \tag{4}$$

using a local rectangular time window centered at (t_1,t_2) with size N.
For any t_1 and t_2 we obtain that

$$\boldsymbol{C}^{\underline{S}}(t_1,t_2) = \frac{\pi^2}{N^2} \sum_{j_1=-N}^{N-1} \sum_{j_2=-N}^{N-1} \breve{\boldsymbol{f}}^{\underline{S}}_{t_1,t_2}\left(\omega^N_{j_1},\omega^N_{j_2}\right) e^{i\left(\omega^N_{j_1} t_1 - \omega^N_{j_2} t_2\right)}, \tag{5}$$

where $w^N_j := \frac{j\pi}{N}$, $j = -N,\ldots,N-1$ are the Fourier frequencies of the local rectangular time window.
When $\{\boldsymbol{X}^{\underline{S}}_t\}$ is a family of spatial time-harmonizable processes with spectrum $\boldsymbol{f}^{\underline{S}}(\omega_1,\omega_2)$ one can easily verify that

$$\begin{aligned}
&\breve{\boldsymbol{f}}^{\underline{S}}_{t_1,t_2}(\omega_1,\omega_2) \\
&= \frac{1}{4\pi^2} \int_{-\pi}^{\pi}\int_{-\pi}^{\pi} D_N(\omega'_1)\overline{D_N(\omega'_2)} e^{i\left(\omega'_1 t_1 - \omega'_2 t_2\right)} \boldsymbol{f}^{\underline{S}}\left(\omega_1+\omega'_1, \omega_2+\omega'_2\right) d\omega'_1 d\omega'_2,
\end{aligned}$$

where $D_N(0) = 2N$ and $D_N(\omega) = \frac{2i\sin(\omega N)}{e^{i\omega}-1}$ otherwise. Furthermore, if for each t_1 and t_2,

$$\sum_{(t_1,t_2)\in\mathbb{Z}^2} \left|\boldsymbol{C}^{\underline{S}}(t_1,t_2)\right| < \infty,$$

then

$$\lim_{N\to\infty} \breve{\boldsymbol{f}}^{\underline{S}}_{t_1,t_2}(\omega_1,\omega_2) = \boldsymbol{f}^{\underline{S}}(\omega_1,\omega_2).$$

2.3 The observations

In the following, we consider replicates $\{\mathbf{X}_t^{\underline{S},r}\}$, $r \in \mathbb{N}^*$, of a spatial zero-mean second order process $\{\mathbf{X}_t^{\underline{S}}\}$. This means that the processes $\{\mathbf{X}_t^{\underline{S},r}\}$ have the same distribution as $\{\mathbf{X}_t^{\underline{S}}\}$. Here the process is not necessarily time-harmonizable. From now on, we assume that the replicates are dependent, more precisely, that the family of processes $\{\mathbf{X}_t^{\underline{S},r}\}$, $r \in \mathbb{N}^*$, is nonstationary with respect to t and stationary with respect to r.
Consequently, we denote

$$\boldsymbol{C}^{\underline{S}}(t_1,t_2) := \mathrm{Cov}\big(\boldsymbol{X}_{t_1}^{\underline{S},1}, \boldsymbol{X}_{t_2}^{\underline{S},1}\big) = \mathrm{Cov}\big(\boldsymbol{X}_{t_1}^{\underline{S},r}, \boldsymbol{X}_{t_2}^{\underline{S},r}\big) \tag{6}$$

for any positive integer r, and

$$\breve{\boldsymbol{f}}_{t_1,t_2}^{\underline{S}}(\omega_1,\omega_2) := \frac{1}{4\pi^2} \sum_{k_1=t_1-N}^{t_1+N-1} \sum_{k_2=t_2-N}^{t_2+N-1} \boldsymbol{C}^{\underline{S}}(k_1,k_2)\; e^{-i(\omega_1 k_1 - \omega_2 k_2)}. \tag{7}$$

Then

$$\boldsymbol{C}^{\underline{S}}(t_1,t_2) = \frac{\pi^2}{N^2} \sum_{j_1=-N}^{N-1} \sum_{j_2=-N}^{N-1} \breve{\boldsymbol{f}}_{t_1,t_2}^{\underline{S}}\big(\omega_{j_1}^N, \omega_{j_2}^N\big) e^{i\left(\omega_{j_1}^N t_1 - \omega_{j_2}^N t_2\right)},$$

where $w_j^N := \frac{j\pi}{N}$, $j = -N, \ldots, N-1$.
The r-th replicate is observed at time instants $0, \ldots, T-1$ and at $S_1 \times S_2$ different spatial locations. Hence

$$\begin{aligned} \{\mathbf{X}^{\underline{S},r}\} &= \{\mathbf{X}_t^{\underline{S},r}, t = 0, \ldots, T-1\} \\ &= \big\{X_{\underline{s},t}^{\underline{S},r}, t = 0, \ldots, T-1,\ \underline{s} \in \{1, \ldots, S_1\} \times \{1, \ldots, S_2\}\big\}, \end{aligned}$$

where $\underline{S} = (S_1, S_2) \in \mathbb{N}^{*2}$. For the sake of simplicity we set $\mathbf{X}_t^{\underline{S},r} = \mathbf{0}_{S_1 \times S_2}$ (the null $S_1 \times S_2$-matrix) for $t \notin \{0, \ldots, T-1\}$.

In the following, we study the asymptotic behavior of the localized Loève spectrum $\breve{\boldsymbol{f}}_{t_1,t_2}^{\underline{S}}(\omega_1,\omega_2)$. For that purpose we introduce the rescaled spatiotemporal spectrum and we construct its estimator. All asymptotic results are obtained as S_1, S_2, T, R go to ∞. The time window size N can be fixed or going to ∞.

2.4 Assumptions

To obtain the asymptotic results we assume the following conditions.

(L) *Rescaling conditions.* There exists a function $f : [0,1]^6 \times (-\pi,\pi]^2 \to \mathbb{C}$ and positive constants L and Q such that

$$\begin{aligned}&\left|f_{\underline{u}_1,\underline{u}_2,\tau_1,\tau_2}(\omega_1,\omega_2) - f_{\underline{u}_3,\underline{u}_4,\tau_3,\tau_4}(\omega_1,\omega_2)\right| \\ &\quad\leq L\left(\|\underline{u}_1 - \underline{u}_3\| + \|\underline{u}_2 - \underline{u}_4\| + |\tau_1 - \tau_3| + |\tau_2 - \tau_4|\right)\end{aligned} \tag{8}$$

for any $\underline{u}_1, \underline{u}_2, \underline{u}_3, \underline{u}_4, \in [0,1]^2$, $\tau_1, \tau_2 \in [0,1]$ and $\omega_1, \omega_2 \in (-\pi, \pi]$ and

$$\left|\breve{f}^{\underline{S}}_{\underline{s}_1,\underline{s}_2,t_1,t_2}(\omega_1,\omega_2) - f_{\ddot{\underline{s}}_1,\ddot{\underline{s}}_2,\ddot{t}_1,\ddot{t}_2}(\omega_1,\omega_2)\right| \leq Q\left(\frac{1}{S_1} + \frac{1}{S_2} + \frac{1}{T}\right), \tag{9}$$

where $\underline{s}_i := (s_{i,1}, s_{i,2})$, $\ddot{\underline{s}}_i := (s_{i,1}/S_1, s_{i,2}/S_2), \ddot{t}_i := t_i/T, i = 1,2$ for $N \leq t_1, t_2 \leq T - N$. Inequality (9) is assumed to be true for all S_1, S_2 and T large enough, and for N fixed or sufficiently large, as the case may be.
Hereafter, $f_{\underline{u}_1,\underline{u}_2,\tau_1,\tau_2}(\omega_1,\omega_2)$ is called the **rescaled Loève spectrum**

(SR) The replications $\{\mathbf{X}_t^{\underline{S},r}\}$, $r \in \mathbb{N}^*$ have the same distribution and are stationary with respect to r.

(MR) *Mixing property for the replicates:* The family $\{\boldsymbol{X}^{\underline{S},r}\}$, $r \in \mathbb{N}^*$, $\underline{S} \in \mathbb{N}^{*2}$, is α-mixing with respect to r and such that one of the following two conditions holds:
(i) $\sup_{t,\underline{S}} \left|\boldsymbol{X}_t^{\underline{S},1}\right| < C$ almost surely for some finite $C > 0$ and $\sum_\kappa \alpha_X(\kappa) < \infty$,
(ii) $\sup_{t,\underline{S}} \mathrm{E}\left(\left|\boldsymbol{X}_t^{\underline{S},1}\right|^{4+\delta}\right) < \infty$ and $\sum_\kappa \alpha_X(\kappa)^{\delta/(4+\delta)} < \infty$ for some $\delta > 0$.
The mixing coefficients are defined as follows

$$\alpha_X(\kappa) := \sup_r \sup_{\underline{S}} \sup_{\substack{A \in \mathcal{F}_r(\underline{S}) \\ B \in \mathcal{F}^{r+\kappa}(\underline{S})}} \left|\mathrm{P}(A \cap B) - \mathrm{P}(A)\mathrm{P}(B)\right|,$$

where $\mathcal{F}_r(\underline{S}) := \sigma\left\{X_{\underline{s},t}^{\underline{S},q} : q \leq r, t \in \mathbb{Z} \text{ and all locations } \underline{s}\right\}$ and
$\mathcal{F}^{r+\kappa}(\underline{S}) := \sigma\left\{X_{\underline{s},t}^{\underline{S},q} : q \geq r+\kappa, t \in \mathbb{Z} \text{ and all locations } \underline{s}\right\}$.

In order to state the asymptotic covariance of our estimator we consider an additional rescaling assumption, which is a generalization of the condition (L) to the four-dimensional spectrum. Denote $\boldsymbol{t} := (t_1, t_2, t_3, t_4) \in \mathbb{Z}^4$, $\boldsymbol{\tau} := (\tau_1, \tau_2, \tau_3, \tau_4) \in [0,1]^4$ and $\boldsymbol{\omega} := (\omega_1, \omega_2, \omega_3, \omega_4) \in (-\pi, \pi]^4$. Moreover, for $\underline{s}_j \in \mathbb{N}^{*2}$ and $\underline{u}_j \in [0,1]^2$, $j = 1, \ldots, 4$, let $\boldsymbol{s} := (\underline{s}_1, \underline{s}_2, \underline{s}_3, \underline{s}_4) \in \mathbb{N}^{*8}$ and $\boldsymbol{u} := (\underline{u}_1, \underline{u}_2, \underline{u}_3, \underline{u}_4) \in [0,1]^8$. Under the stationary condition (SR) the covariance

$$C_{\boldsymbol{s},\boldsymbol{t}}^{\underline{S},\kappa} := \mathrm{Cov}\left(X_{\underline{s}_1,t_1}^{\kappa+r} X_{\underline{s}_2,t_2}^{\kappa+r}\,,\, X_{\underline{s}_3,t_3}^{r} X_{\underline{s}_4,t_4}^{r}\right)$$

does not depend on $r \geq \max\{0, -\kappa\}$, for any $\kappa \in \mathbb{Z}$. Then define

$$\breve{f}^{\underline{S},\kappa}_{\boldsymbol{s},\boldsymbol{t}}(\boldsymbol{\omega}) := \frac{1}{16\pi^4} \sum_{k_1=t_1-N}^{t_1+N-1} \sum_{k_2=t_2-N}^{t_2+N-1} \sum_{k_3=t_3-N}^{t_3+N-1} \sum_{k_4=t_4-N}^{t_4+N-1} C^{\underline{S},\kappa}_{\boldsymbol{s},\boldsymbol{k}} e^{-i(\omega_1 k_1 - \omega_2 k_2 - \omega_3 k_3 + \omega_4 k_4)}.$$

The rescaling assumption is as follows.

(LR) *Rescaling condition for the replicates.* There exist functions $f^\kappa : [0,1]^{12} \times (-\pi, \pi]^4 \to \mathbb{C}$, $\kappa \in \mathbb{N}^*$, and some positive constants L and Q such that for each $\boldsymbol{u_i} \in [0,1]^8$, $\boldsymbol{\tau_i} \in [0,1]^4$, $\boldsymbol{\omega} \in (-\pi, \pi]^4$, $i = 1, 2$ and each $\kappa \in \mathbb{N}^*$,

$$\left| f^\kappa_{\boldsymbol{u_1},\boldsymbol{\tau_1}}(\boldsymbol{\omega}) - f^\kappa_{\boldsymbol{u_2},\boldsymbol{\tau_2}}(\boldsymbol{\omega}) \right| \leq L \sum_{j=1}^{4} \left(\|\underline{u}_{j,1} - \underline{u}_{j,2}\| + |\tau_{j,1} - \tau_{j,2}| \right) \tag{10}$$

and

$$\left| \breve{f}^{\underline{S},\kappa}_{\boldsymbol{s},\boldsymbol{t}}(\boldsymbol{\omega}) - f^\kappa_{\ddot{\boldsymbol{s}},\ddot{\boldsymbol{t}}}(\boldsymbol{\omega}) \right| \leq Q \left(\frac{1}{S_1} + \frac{1}{S_2} + \frac{1}{T} \right), \tag{11}$$

where $\underline{s}_j = (s_{j,1}, s_{j,2})$, $\ddot{\underline{s}}_j = (s_{j,1}/S_1, s_{j,2}/S_2), \ddot{t}_j = t_j/T, j = 1, 2, 3, 4$ and for $N \leq t_1, t_2, t_3, t_4 \leq T - N$.
Furthermore, assume that

$$\sum_{\kappa \in \mathbb{Z}} \left| f^\kappa_{\boldsymbol{u},\boldsymbol{\tau}}(\boldsymbol{\omega}^{\boldsymbol{M}}_{\boldsymbol{l}}) \right| < \infty, \tag{12}$$

for the Fourier frequencies $\boldsymbol{\omega}^{\boldsymbol{M}}_{\boldsymbol{l}} = (\omega^M_{l_1}, \ldots, \omega^M_{l_4})$ and $\omega^M_{l_i} = \frac{l_i \pi}{M}$, $l_i = -M, \ldots, M - 1\}, i = 1, \ldots, 4$, where the integer $M > 0$ is fixed and $N = nM$. Inequality (11) is assumed to be true for all S_1, S_2 and T sufficiently large, and for N fixed or sufficiently large, as the case may be.

Remark 2.1.

1. Under conditions (L) and (LR) the functions $f_{\underline{u}_1,\underline{u}_2,\tau_1,\tau_2}(\omega_1, \omega_2)$ and $f^\kappa_{\boldsymbol{u},\boldsymbol{\tau}}(\boldsymbol{\omega})$ are L-Lipschitz-continuous in space and time components uniformly with respect to the frequencies $\omega_1, \ldots, \omega_4$ and the shift κ between replicates.

2. *Identifiability.* In condition (L), relation (9) is assumed to be true for all S_1, S_2 and T sufficiently large. Hence, if $f_{\underline{u}_1,\underline{u}_2,\tau_1,\tau_2}(\omega_1, \omega_2)$ exists then it is unique. Similarly, under condition (LR) the function $f^\kappa_{\boldsymbol{u},\boldsymbol{\tau}}(\boldsymbol{\omega})$ is unique.

3. When we assume that $N \to \infty$, then the rescaled Loève spectrum $f_{\underline{u}_1,\underline{u}_2,\tau_1,\tau_2}(\omega_1,\omega_2)$ does not depend on N. Of course, if N is assumed to be fixed then $f_{\underline{u}_1,\underline{u}_2,\tau_1,\tau_2}(\omega_1,\omega_2)$ may depend on N.

4. *Example for condition (L).* Let $\{\boldsymbol{X}_t^{\underline{S}}\}$ be a spatial time-harmonizable process with the Loève spectrum of the form $f^{\underline{S}}_{\underline{s}_1,\underline{s}_2}(\omega_1,\omega_2) = A^{\underline{S}}(\underline{s}_1,\underline{s}_2)\,\phi(\omega_1,\omega_2)$, where the function $\phi(\omega_1,\omega_2)$ is bounded, say $|\phi(\omega_1,\omega_2)| \leq c$, $c>0$, and

$$\left|A^{\underline{S}}(\underline{s}_1,\underline{s}_2) - A(\ddot{\underline{s}}_1,\ddot{\underline{s}}_2)\right| \leq \frac{Q}{c}\left(\frac{1}{S_1}+\frac{1}{S_2}\right)$$

for some (L/c)-Lipschitz-continuous function $A:[0,1]^4 \to \mathbb{C}$. Then assumption (L) is fulfilled with $f_{\underline{\ddot{s}}_1,\underline{\ddot{s}}_2,\ddot{t}_1,\ddot{t}_2}(\omega_1,\omega_2) = A(\underline{\ddot{s}}_1,\underline{\ddot{s}}_2)\,\phi(\omega_1,\omega_2)$. (See also Ombao et al. [2008])

5. The α-mixing function α_X is a weak dependence measure. Hence, replicated processes $\{\boldsymbol{X}^{\underline{S},r_1}\}$ and $\{\boldsymbol{X}^{\underline{S},r_2}\}$ that are close to each other, i.e. such that the distance $\kappa := |r_1 - r_2|$ between replications is small, can be dependent, while when κ is large, they are almost independent. The replicates are M-dependent, $M \geq 1$, if and only if $\alpha_X(\kappa) = 0$ for any $\kappa \geq M$. This generalizes the modeling assumptions in [Gorrostieta et al., 2019], where the replicates are assumed to be independent, that is $\alpha_X(\kappa) = 0$ for any $\kappa \neq 0$. For properties and examples of other dependence measures, we refer the reader to [Doukhan, 1994].

6. *Gaussian framework.* In Section 4, we present the results for a Gaussian process. In this case, the mixing condition is useless, and the condition (LR) is replaced by (LGR). Then we give an expression for the four-dimensional rescaled spectrum $f^{\kappa}_{\boldsymbol{u},\boldsymbol{\tau}}(\boldsymbol{\omega})$ in terms of the two-dimensional rescaled spectrum. See relation (24).

In the following, we provide the results in two cases: N fixed and $N \to \infty$, that is n fixed and $n \to \infty$ for M fixed with $N = nM$. The integer M being defined below according to the frequency resolution. The case $N \to \infty$ denotes that we consider infinitely many time points around each instant t.

2.5 Estimator of the rescaled Loève spectrum

In this section we introduce an estimation procedure for the rescaled Loève spectrum $f_{\underline{u}_1,\underline{u}_2,\tau_1,\tau_2}(\omega_1,\omega_2)$. For that purpose, we first define two kernel functions that we use for rescaling in space and time. To simplify the presentation, let us consider two non-negative functions $w, W : \mathbb{R} \to [0,\infty)$ and two positive numbers h and $\hbar$. We define

$$w_{\underline{u}}(\underline{s}) := \frac{1}{S_1 S_2 h^2}\, w\left(\frac{u_1 - s_1/S_1}{h}\right) w\left(\frac{u_2 - s_2/S_2}{h}\right),$$

and

$$W_\tau(t) := \frac{1}{T\hbar} W\left(\frac{\tau - t/T}{\hbar}\right)$$

where $\underline{u} = (u_1, u_2) \in [0,1]^2$, $\underline{s} = (s_1, s_2) \in \{1, \ldots, S_1\} \times \{1, \ldots, S_2\}$, $\tau \in [0,1]$ and $t \in \mathbb{N}$. Notice that the kernel function $w_{\underline{u}}(\underline{s})$ depends on $\underline{S}$ and h, and $W_\tau(t)$ depends on T and $\hbar$. In the following, we always assume the following condition on $W(\cdot)$ and $w(\cdot)$.

(KS) The kernel functions $w(\cdot) : \mathbb{R} \to [0, \infty)$ and $W(\cdot) : \mathbb{R} \to [0, \infty)$ are symmetric nonnegative with support contained in $[-1, 1]$ and such that $\int_{-1}^{1} w(u)du = \int_{-1}^{1} W(u)du = 1$. Moreover, they are piecewise Lipschitz-continuous in the sense that there exist $k, k' \in \mathbb{N}^*$, $-1 = \upsilon_1 < \cdots < \upsilon_k = 1$ and $-1 = \tau_1 < \cdots < \tau_{k'} = 1$ such that $w(\cdot)$ and $W(\cdot)$ are Lipschitz-continuous on each interval $(\upsilon_j, \upsilon_{j+1})$, $1 \leq j \leq k-1$ and $(\tau_{j'}, \tau_{j'+1})$, $1 \leq j' \leq k' - 1$, respectively.

Note that under the condition (KS) the kernel functions $w(\cdot)$ and $W(\cdot)$ are bounded. It holds for instance for rectangular and triangular kernels.

Now we define the dual-frequency periodogram of the r-th replicate for the spatial locations $\underline{s}_1, \underline{s}_2$ and the instants t_1, t_2 at frequencies ω_1, ω_2 and over a time window of size N as

$$I^r_{\underline{s}_1,\underline{s}_2,t_1,t_2}(\omega_1, \omega_2) := \frac{1}{4\pi^2} d^r_{\underline{s}_1,t_1}(\omega_1)\, \overline{d^r_{\underline{s}_2,t_2}(\omega_2)},$$

where

$$d^r_{\underline{s},t}(\omega) := \sum_{k=t-N}^{t+N-1} X^{\underline{S},r}_{\underline{s},k} e^{-i\omega k} = \sum_{k=-N}^{N-1} X^{\underline{S},r}_{\underline{s},k+t} e^{-i\omega(k+t)}$$

is the discrete Fourier transform of the r-th replicate for the spatial location $\underline{s}$ around the instant t. Recall that we set $X^r_{\underline{s},k} = 0$ for $k \notin \{0, \ldots, T-1\}$.
Then the estimator of the local Loève spectrum is defined as the average of the dual-frequency periodograms of replicates i.e.,

$$\hat{f}_{\underline{s}_1,\underline{s}_2,t_1,t_2}(\omega_1, \omega_2) := \frac{1}{R} \sum_{r=1}^{R} I^r_{\underline{s}_1,\underline{s}_2,t_1,t_2}(\omega_1, \omega_2).$$

Finally, the estimator of the rescaled Loève spectrum $f_{\underline{u}_1,\underline{u}_2,\tau_1,\tau_2}(\omega_1, \omega_2)$ is given by

$$\begin{aligned}&\widetilde{f}_{\underline{u}_1,\underline{u}_2,\tau_1,\tau_2}(\omega_1, \omega_2) \\ &\quad := \sum_{t_1} \sum_{t_2} \sum_{\underline{s}_1} \sum_{\underline{s}_2} W_{\tau_1}(t_1) W_{\tau_2}(t_2) w_{\underline{u}_1}(\underline{s}_1) w_{\underline{u}_2}(\underline{s}_2) \hat{f}_{\underline{s}_1,\underline{s}_2,t_1,t_2}(\omega_1, \omega_2). \end{aligned} \tag{13}$$

The rescaled coherence is defined as

$$\rho_{\underline{u}_1,\underline{u}_2,\tau_1,\tau_2}(\omega_1,\omega_2) := \frac{\left|f_{\underline{u}_1,\underline{u}_2,\tau_1,\tau_2}(\omega_1,\omega_2)\right|^2}{f_{\underline{u}_1,\underline{u}_1,\tau_1,\tau_1}(\omega_1,\omega_1)\, f_{\underline{u}_2,\underline{u}_2,\tau_2,\tau_2}(\omega_2,\omega_2)}, \tag{14}$$

and its estimator is given by

$$\widetilde{\rho}_{\underline{u}_1,\underline{u}_2,\tau_1,\tau_2}(\omega_1,\omega_2) := \frac{\left|\widetilde{f}_{\underline{u}_1,\underline{u}_2,\tau_1,\tau_2}(\omega_1,\omega_2)\right|^2}{\widetilde{f}_{\underline{u}_1,\underline{u}_1,\tau_1,\tau_1}(\omega_1,\omega_1)\, \widetilde{f}_{\underline{u}_2,\underline{u}_2,\tau_2,\tau_2}(\omega_2,\omega_2)}. \tag{15}$$

Due to the limitation of the frequency resolution capacity in the real life experiment, in the sequel we consider the convergence of the estimator $\widetilde{f}_{\underline{u}_1,\underline{u}_2,\tau_1,\tau_2}(\omega_1,\omega_2)$ for a finite number of Fourier frequencies $\omega_l^M := \frac{l\pi}{M}$, $-M \le l \le M-1$, where $M > 1$ is some fixed integer. Furthermore, in order to ensure the identifiability of the frequencies, we take the window size N equal to an integer multiple of M: $N = nM$.
This choice of modeling allows us to derive a more accessible asymptotic theory presented in Section 3. Moreover, it is motivated by our real data application for which we typically consider a finite number of frequency bands of interest. In particular, we consider the sets of Fourier frequencies $\Omega_i := \left\{\omega_j^M : L_i \le j \le L_i + l_i - 1\right\}$, for some $l_i \ge 1$, $i = 1, 2$. Then the estimator is computed as an average over the frequencies

$$\widetilde{f}_{\underline{u}_1,\underline{u}_2,\tau_1,\tau_2}(\Omega_1,\Omega_2) := \frac{1}{l_1 l_2} \sum_{j_1=L_1}^{L_1+l_1-1} \sum_{j_2=L_2}^{L_2+l_2-1} \widetilde{f}_{\underline{u}_1,\underline{u}_2,\tau_1,\tau_2}\left(\omega_{j_1}^M, \omega_{j_2}^M\right). \tag{16}$$

3 Main results

Below we state some asymptotic properties of our estimation procedure like convergence in quadratic mean and asymptotic normality. All the proofs are deferred to the companion document [Aston et al., 2022].
From now on any complex number z is treated as a vector of its real and imaginary parts, i.e., $z = (\Re z, \Im z)'$.

Theorem 3.1. *(Convergence in quadratic mean)*
Let $M \ge 1$, $\underline{u}_1, \underline{u}_2 \in (0,1)^2$ and $\tau_1, \tau_2 \in (0,1)$ be fixed. Assume that the assumptions (L) and (MR) hold. Then

$$\lim_{R\to\infty} \widetilde{f}_{\underline{u}_1,\underline{u}_2,\tau_1,\tau_2}\left(\omega_{l_1}^M, \omega_{l_2}^M\right) = f_{\underline{u}_1,\underline{u}_2,\tau_1,\tau_2}\left(\omega_{l_1}^M, \omega_{l_2}^M\right) \qquad \textit{in quadratic mean,}$$

for the Fourier frequencies $\omega_{l_i}^M = \frac{l_i\pi}{M}$, $l_i = -M, \dots, M-1$, $i = 1, 2$, *provided that* $N = nM$, $n^4R^{-1} \to 0$, $h^2S_1, h^2S_2, \hbar^2T \to \infty$ *and* $n^2(h+\hbar), n^3T^{-1} \to 0$ *as* $T, S_1, S_2, R \to \infty, h, \hbar \to 0$ *independently of the behavior of* $n \geq 1$.

Below we express the asymptotic covariance matrix of the estimator $\widetilde{f}_{\underline{u}_1,\underline{u}_2,\tau_1,\tau_2}$.

Lemma 3.1. *Let* $M \geq 1$, $\underline{u}_i \in (0,1)^2$, $\tau_i \in (0,1)$ *and the Fourier frequencies* $\omega_{l_i}^M$ *be fixed,* $i = 1, 2, 3, 4$. *Assume that the assumptions (SR) and (LR) hold. Then*

$$\lim_{R\to\infty} R\operatorname{Cov}\left(\widetilde{f}_{\underline{u}_1,\underline{u}_2,\tau_1,\tau_2}\left(\omega_{l_1}^M, \omega_{l_2}^M\right), \widetilde{f}_{\underline{u}_3,\underline{u}_4,\tau_3,\tau_4}\left(\omega_{l_3}^M, \omega_{l_4}^M\right)\right) = \sum_{\kappa\in\mathbb{Z}} f_{\boldsymbol{u},\boldsymbol{\tau}}^{\kappa}\left(\boldsymbol{\omega}_{\boldsymbol{l}}^{\boldsymbol{M}}\right),$$

provided that $N = nM$, $h^2S_1, h^2S_2, \hbar^2T \to \infty$, $n^4(h+\hbar), n^5T^{-1} \to 0$ *as* $T, S_1, S_2, R \to \infty$, $h, \hbar \to 0$.

Before we formulate the multivariate central limit theorem we introduce some additional notation. Let

$$\boldsymbol{f} := \left(\left(f_{\underline{u}_{1,1},\underline{u}_{2,1},\tau_{1,1},\tau_{2,1}}\left(\omega_{1,1},\omega_{2,1}\right)\right)', \dots, \left(f_{\underline{u}_{1,k},\underline{u}_{2,k},\tau_{1,k},\tau_{2,k}}\left(\omega_{1,k},\omega_{2,k}\right)\right)'\right)',$$

and

$$\widetilde{\boldsymbol{f}} := \left(\left(\widetilde{f}_{\underline{u}_{1,1},\underline{u}_{2,1},\tau_{1,1},\tau_{2,1}}\left(\omega_{1,1},\omega_{2,1}\right)\right)', \dots, \left(\widetilde{f}_{\underline{u}_{1,k},\underline{u}_{2,k},\tau_{1,k},\tau_{2,k}}\left(\omega_{1,k},\omega_{2,k}\right)\right)'\right)',$$

where k is some positive integer, $\underline{u}_{i,j} \in (0,1)^2$, $\tau_{i,j} \in (0,1)$, $\omega_{i,j} = \omega_{l_{i,j}}^M = \frac{l_{i,j}\pi}{M}$, $i = 1, 2$ and $j = 1, \dots, k$.

Now we state the asymptotic normality of the estimator.

Theorem 3.2. *Assume that the assumptions (L), (SR), (MR) and (LR) hold. Then*

$$\lim_{R\to\infty} \mathcal{L}\left(\sqrt{R}\left(\widetilde{\boldsymbol{f}} - \boldsymbol{f}\right)\right) = \mathcal{N}_{2k}\left(0, \boldsymbol{\Sigma}_{2k}\right),$$

provided that
(i) either $N = nM$ *is a constant,* $T, S_1, S_2, R \to \infty, h, \hbar \to 0$ *with* $Rh^{-4}(S_1^{-2}+S_2^{-2}), R\hbar^{-4}T^{-2}$, $R(h^2+\hbar^2) \to 0$;
(ii) or $N = nM \to \infty$, $T, S_1, S_2, R \to \infty, h, \hbar \to 0$ *with* $Rh^{-4}(S_1^{-2}+S_2^{-2}), R\hbar^{-4}T^{-2}, Rn^4(h^2+\hbar^2), Rn^6T^{-2} \to 0$, *and the additional condition*

$$\sum_t \left|X_{\underline{s}_i,t}^{\underline{S},1}\right| \leq C \tag{17}$$

almost surely, or

$$\sum_t \mathrm{E}\left(\left|X^{\underline{S},1}_{\underline{s}_i,t}\right|^{4+\delta}\right)^{1/(4+\delta)} \leq C \tag{18}$$

for some finite $C > 0$ which does not depend on the locations. The elements of the covariance $(2k \times 2k)$-matrix $\mathbf{\Sigma}_{2k}$ can be calculated from Lemma 3.1.

Remark 3.1. *When $N \to \infty$, conditions (17) and (18) can be replaced by more subtle assumptions. For the sake of clarity, this technical remark is detailed only in the companion document. See conditions (ii) in Proposition 1 in the companion document [Aston et al., 2022] and to the subsequent remarks.*

Theorem 3.2 is crucial to study the behavior of $\widetilde{f}_{\underline{u}_1,\underline{u}_2,\tau_1,\tau_2}(\Omega_1,\Omega_2)$ given by the equation (16).

Corollary 3.1. *Under conditions of Theorem 3.2, the estimator $\tilde{\rho}$ of the rescaled spatiotemporal coherence ρ, defined respectively by (15) is asymptotically normal i.e.,*

$$\lim_{R\to\infty} \mathcal{L}\left(\sqrt{R}\left(\tilde{\rho}_{\underline{u}_1,\underline{u}_2,\tau_1,\tau_2}(\omega_1,\omega_2) - \rho_{\underline{u}_1,\underline{u}_2,\tau_1,\tau_2}(\omega_1,\omega_2)\right)\right) = \mathcal{N}(0,\gamma^2), \tag{19}$$

where the Fourier frequencies $\omega_i = \omega_{l_i}^M$ with $l_i \in \{M,\ldots,M-1\}$, $i = 1,2$ and provided that $f_{\underline{u}_1,\underline{u}_1,\tau_1,\tau_1}(\omega_1,\omega_1) \times f_{\underline{u}_2,\underline{u}_2,\tau_2,\tau_2}(\omega_2,\omega_2) \neq 0$.
Here $\gamma^2 = (\nabla^{(\omega_1,\omega_2)}_{\underline{u}_1,\underline{u}_2,\tau_1,\tau_2})\mathbf{\Sigma}_6(\nabla^{(\omega_1,\omega_2)}_{\underline{u}_1,\underline{u}_2,\tau_1,\tau_2})'$, where ∇ denotes the gradient operator. The covariance 6×6 matrix $\mathbf{\Sigma}_6$ is given in Theorem 3.2 for $k = 3$, $\tau_{1,1} = \tau_{2,1} = \tau_{1,3} = \tau_1$, $\tau_{1,2} = \tau_{2,2} = \tau_{2,3} = \tau_2$, $\underline{u}_{1,1} = \underline{u}_{2,1} = \underline{u}_{1,3} = \underline{u}_1$, $\underline{u}_{1,2} = \underline{u}_{2,2} = \underline{u}_{2,3} = \underline{u}_2$, $\omega_{1,1} = \omega_{2,1} = \omega_{1,3} = \omega_1$, and $\omega_{1,2} = \omega_{2,2} = \omega_{2,3} = \omega_2$. Moreover,

$$\begin{aligned}
&\nabla^{(\omega_1,\omega_2)}_{\underline{u}_1,\underline{u}_2,\tau_1,\tau_2} \\
&= \left(\frac{-\left|f_{\underline{u}_1,\underline{u}_2,\tau_1,\tau_2}(\omega_1,\omega_2)\right|^2}{\left(f_{\underline{u}_1,\underline{u}_1,\tau_1,\tau_1}(\omega_1,\omega_1)\right)^2 f_{\underline{u}_2,\underline{u}_2,\tau_2,\tau_2,}(\omega_2,\omega_2)}, 0, \frac{-\left|f_{\underline{u}_1,\underline{u}_2,\tau_1,\tau_2}(\omega_1,\omega_2)\right|^2}{f_{\underline{u}_1,\underline{u}_1,\tau_1,\tau_1}(\omega_1,\omega_1)\left(f_{\underline{u}_2,\underline{u}_2,\tau_2,\tau_2}(\omega_2,\omega_2)\right)^2},\right. \\
&\qquad \left. 0, \frac{2\Re f_{\underline{u}_1,\underline{u}_2,\tau_1,\tau_2}(\omega_1,\omega_2)}{f_{\underline{u}_1,\underline{u}_1,\tau_1,\tau_1}(\omega_1,\omega_1) f_{\underline{u}_2,\underline{u}_2,\tau_2,\tau_2}(\omega_2,\omega_2)}, \frac{2\Im f_{\underline{u}_1,\underline{u}_2,\tau_1,\tau_2}(\omega_1,\omega_2)}{f_{\underline{u}_1,\underline{u}_1,\tau_1,\tau_1}(\omega_1,\omega_1) f_{\underline{u}_2,\underline{u}_2,\tau_2,\tau_2}(\omega_2,\omega_2)}\right)'.
\end{aligned}$$

Bootstrap approach

Using Corollary 3.1 one may construct confidence interval for the spatiotemporal dual-frequency coherence $\rho_{\underline{u}_1,\underline{u}_2,\tau_1,\tau_2}(\omega_1,\omega_2)$. However, since the asymptotic variance γ^2 depends on unknown parameters, it is in practice very difficult to estimate. Thus, we

present below a bootstrap approach that allows to obtain consistent confidence intervals for $\rho_{\tau_1,\tau_2,\underline{u}_1,\underline{u}_2}(\omega_1,\omega_2)$.

Let us recall that we have R replicates $\{\boldsymbol{X}^{(r)}\} = \{\boldsymbol{X}_t^{\underline{S},r}\} = \{X_{\underline{s},t}^{\underline{S},r}, t \in \mathbb{Z}, \underline{s} \in \{1,\dots,S_1\} \times \{1,\dots,S_2\}\}$, $r = 1,\dots,R$. The process $\left\{X_{\underline{s},t}^{\underline{S},r}\right\}$ is stationary in r and nonstationary in t. We will bootstrap our observations in replicates not in time. For that purpose we use the CBB (see Politis and Romano [1992]). The CBB is a modification of the Moving Block Bootstrap method [Künsch, 1989, Liu and Singh, 1992], which allows to reduce bias of the bootstrap estimator. Below we present how to adapt the CBB algorithm to our problem. Let B_i, $i = 1,\dots,R$ be the block of replicates from our sample $\left(\boldsymbol{X}^{(1)},\dots,\boldsymbol{X}^{(R)}\right)$, that starts with replicate $\boldsymbol{X}^{(i)}$ and has the length $b \in \mathbb{N}$, i.e.

$$B_i := \left(\boldsymbol{X}^{(i)},\dots,\boldsymbol{X}^{(i+b-1)}\right).$$

If $i+b-1 > R$ then the missing part of the block is taken from the beginning of the sample and we get

$$B_i = \left(\boldsymbol{X}^{(i)},\dots,\boldsymbol{X}^{(R)},\boldsymbol{X}^{(1)},\dots,\boldsymbol{X}^{(b-R+i-1)}\right)$$

for $i = R-b+2,\dots,R$.

CBB algorithm

1. Choose a block size $b < R$. Then our sample $\left(\boldsymbol{X}^{(1)},\dots,\boldsymbol{X}^{(R)}\right)$ can be divided into l blocks of length b and the remaining part is of length r, i.e. $R = lb+r$, $R = 0,\dots,b-1$.
2. From the set $\{B_1,\dots,B_R\}$ choose randomly with replacement $l+1$ blocks.
3. Join the selected $l+1$ blocks $(B_1^*,\dots,B_{l+1}^*)$ and take the first R observations to get the bootstrap sample $\left(\boldsymbol{X}^{*(1)},\dots,\boldsymbol{X}^{*(R)}\right)$ of the same length as the original one.

We apply the CBB to get bootstrap estimators of $f_{\underline{u}_1,\underline{u}_2,\tau_1,\tau_2}(\omega_1,\omega_2)$ and $\rho_{\underline{u}_1,\underline{u}_2,\tau_1,\tau_2}(\omega_1,\omega_2)$ and finally to be able to construct confidence intervals for these characteristics. We use the bootstrap algorithm described above. The bootstrap version of $\widetilde{f}_{\underline{u}_1,\underline{u}_2,\tau_1,\tau_2}(\omega_1,\omega_2)$ is given by

$$\begin{aligned}&\widetilde{f}^*_{\underline{u}_1,\underline{u}_2,\tau_1,\tau_2}(\omega_1,\omega_2)\\ &\quad:= \sum_{t_1}\sum_{t_2}\sum_{\underline{s}_1}\sum_{\underline{s}_2} W_{\tau_1}(t_1)W_{\tau_2}(t_2)w_{\underline{u}_1}(\underline{s}_1)w_{\underline{u}_2}(\underline{s}_2)\hat{f}^*_{\underline{s}_1,\underline{s}_2,t_1,t_2}(\omega_1,\omega_2), \qquad (20)\end{aligned}$$

where

$$\hat{f}^{*}_{\underline{s}_1,\underline{s}_2,t_1,t_2}(\omega_1,\omega_2) := \frac{1}{R}\sum_{r=1}^{R} I^{*,r}_{\underline{s}_1,\underline{s}_2,t_1,t_2}(\omega_1,\omega_2),$$
$$I^{*,r}_{\underline{s}_1,\underline{s}_2,t_1,t_2}(\omega_1,\omega_2) := \frac{1}{4\pi^2} d^{*,r}_{\underline{s}_1,t_1}(\omega_1)\,\overline{d^{*,r}_{\underline{s}_2,t_2}(\omega_2)},$$

and

$$d^{*,r}_{\underline{s},t}(\omega) := \sum_{k=t-N}^{t+N-1} X^{*,r}_{\underline{s},k} e^{-i\omega k}.$$

Below we state the consistency of our bootstrap approach for the spatial time-varying dual-frequency coherence function. The bootstrap estimator of the spatial coherence is defined as

$$\tilde{\rho}^{*}_{\underline{u}_1,\underline{u}_2,\tau_1,\tau_2}(\omega_1,\omega_2) := \frac{\left|\widetilde{f}^{*}_{\underline{u}_1,\underline{u}_2,\tau_1,\tau_2}(\omega_1,\omega_2)\right|^2}{\widetilde{f}^{*}_{\underline{u}_1,\underline{u}_1,\tau_1,\tau_1}(\omega_1,\omega_1)\,\widetilde{f}^{*}_{\underline{u}_2,\underline{u}_2\tau_2,\tau_2}(\omega_2,\omega_2)}.$$

Theorem 3.3. *Under conditions of Theorem 3.2 and assuming that $b^{-1}+R^{-1}b = o(1)$ the CBB is consistent i.e.,*

$$\sup_{x\in\mathbb{R}}\left| P^{*}\left(\sqrt{R}\left(\tilde{\rho}^{*}_{\underline{u}_1,\underline{u}_2,\tau_1,\tau_2}(\omega_1,\omega_2) - \frac{\left(\mathrm{E}^{*}\Re\left(\widetilde{f}^{*}_{\underline{u}_1,\underline{u}_2,\tau_1,\tau_2}(\omega_1,\omega_2)\right)\right)^2 + \left(\mathrm{E}^{*}\Im\left(\widetilde{f}^{*}_{\underline{u}_1,\underline{u}_2,\tau_1,\tau_2}(\omega_1,\omega_2)\right)\right)^2}{\mathrm{E}^{*}\left(\widetilde{f}^{*}_{\underline{u}_1,\underline{u}_1,\tau_1,\tau_1}(\omega_1,\omega_1)\right)\mathrm{E}^{*}\left(\widetilde{f}^{*}_{\underline{u}_2,\underline{u}_2,\tau_2,\tau_2}(\omega_2,\omega_2)\right)}\right) \le x\right)\right.$$
$$\left. - P\left(\sqrt{R}\left(\tilde{\rho}_{\underline{u}_1,\underline{u}_2,\tau_1,\tau_2}(\omega_1,\omega_2)\right) - \rho_{\underline{u}_1,\underline{u}_2,\tau_1,\tau_2}(\omega_1,\omega_2) \le x\right)\right| \xrightarrow{p} 0 \quad as \quad R\longrightarrow\infty \tag{21}$$

for Fourier frequencies $\omega_i = \omega^{M}_{l_i}$ with $l_i \in \{M,\ldots,M-1\}$, $i=1,2$.

Centering of $\tilde{\rho}^{*}_{\underline{u}_1,\underline{u}_2,\tau_1,\tau_2,}(\omega_1,\omega_2)$ may seem surprising. One could expect to use simply $\mathrm{E}^{*}(\tilde{\rho}^{*}_{\underline{u}_1,\underline{u}_2,\tau_1,\tau_2,}(\omega_1,\omega_2))$. But in fact the spatial time-varying dual-frequency coherence function is a function of the rescaled spatiotemporal Loève spectrum and therefore to show convergence (21), one needs first to obtain bootstrap consistency for $\widetilde{f}_{\underline{u}_1,\underline{u}_2,\tau_1,\tau_2}(\omega_1,\omega_2)$, then to generalize this result to a multidimensional case and finally to apply the delta method (see Theorems 2 and 3 in the companion document [Aston et al., 2022]).

While applying block bootstrap a natural question that appears concerns the choice of the block length. In the case of stationary sequences this problem is well investigated (see Lahiri [2003]). It is well known that for the CBB the optimal block length obtained by minimization of the mean squared error of the bootstrap estimator is $b = \mathcal{O}(R^{1/3})$ (see Theorem 5.4 in [Lahiri, 2003]).

4 Gaussian framework

In this section the spatiotemporal random family $\left\{\boldsymbol{X}_t^{\underline{S},r} : t \in \mathbb{Z}, r = 1, \ldots, R\right\}$ is assumed to be Gaussian for any $\underline{S} \in \mathbb{N}^{*2}$ and any $R \in \mathbb{N}^*$. Under the stationarity condition (SR), we have

$$\mathrm{Cov}\big(\boldsymbol{X}_{t_1}^{\underline{S},\kappa+r}, \boldsymbol{X}_{t_2}^{\underline{S},r}\big) = \mathrm{Cov}\big(\boldsymbol{X}_{t_1}^{\underline{S},\kappa+r'}, \boldsymbol{X}_{t_2}^{\underline{S},r'}\big)$$

for any $\kappa \in \mathbb{Z}$ and for any positive integers r and $r' > -\kappa$. Denote

$$\boldsymbol{C}^{\underline{S},\kappa}(t_1, t_2) := \mathrm{Cov}\big(\boldsymbol{X}_{t_1}^{\underline{S},\kappa+r}, \boldsymbol{X}_{t_2}^{\underline{S},r}\big) \tag{22}$$

and define

$$\breve{\boldsymbol{f}}_{t_1,t_2}^{\underline{S},\kappa}(\omega_1, \omega_2) := \frac{1}{4\pi^2} \sum_{k_1=t_1-N}^{t_1+N-1} \sum_{k_2=t_2-N}^{t_2+N-1} \boldsymbol{C}^{\underline{S},\kappa}(k_1, k_2)\ e^{-i(\omega_1 k_1 - \omega_2 k_2)}. \tag{23}$$

Then

$$\boldsymbol{C}^{\underline{S},\kappa}(t_1, t_2) = \frac{\pi^2}{N^2} \sum_{j_1=-N}^{N-1} \sum_{j_2=-N}^{N-1} \breve{\boldsymbol{f}}_{t_1,t_2}^{\underline{S},\kappa}\big(\omega_{j_1}^N, \omega_{j_2}^N\big) e^{i\left(\omega_{j_1}^N t_1 - \omega_{j_2}^N t_2\right)},$$

where $w_j^N := \frac{\pi j}{N}$, $j = -N, \ldots, N-1$ are Fourier frequencies. Moreover, $\boldsymbol{C}^{\underline{S}}(t_1, t_2) = \boldsymbol{C}^{\underline{S},0}(t_1, t_2)$ and $\breve{\boldsymbol{f}}_{t_1,t_2}^{\underline{S}}(\omega_1, \omega_2) = \breve{\boldsymbol{f}}_{t_1,t_2}^{\underline{S},0}(\omega_1, \omega_2)$.

In this Gaussian framework we replace conditions (LR) and (MR) by the following condition on $\breve{\boldsymbol{f}}_{\underline{s}_1,\underline{s}_2,t_1,t_2}^{\underline{S},\kappa}(\omega_1, \omega_2)$ defined by relation (23).

(**LGR**) There exists some positive constant values $L, Q > 0$ and a family of functions $f^\kappa : [0,1]^6 \times (-\pi, \pi]^2 \to \mathbb{C}$, $\kappa \in \mathbb{Z}$, such that

$$\begin{aligned}&\left|f_{\underline{u}_1,\underline{u}_2,\tau_1,\tau_2}^{\kappa}(\omega_1, \omega_2) - f_{\underline{u}_3,\underline{u}_4,\tau_3,\tau_4}^{\kappa}(\omega_1, \omega_2)\right| \\ &\qquad \le L\left(\|\underline{u}_1 - \underline{u}_3\| + \|\underline{u}_2 - \underline{u}_4\| + |\tau_1 - \tau_3| + |\tau_2 - \tau_4|\right)\end{aligned}$$

for any $\underline{u}_1, \underline{u}_2, \underline{u}_3, \underline{u}_4, \in [0,1]^2$, $\tau_1, \tau_2 \in [0,1]$ and $\omega_1, \omega_2 \in (-\pi, \pi]$.

$$\left|\breve{f}_{\underline{s}_1,\underline{s}_2,t_1,t_2}^{\underline{S},\kappa}(\omega_1, \omega_2) - f_{\ddot{\underline{s}}_1,\ddot{\underline{s}}_2,\ddot{t}_1,\ddot{t}_2}^{\kappa}(\omega_1, \omega_2)\right| \le Q\left(\frac{1}{S_1} + \frac{1}{S_2} + \frac{1}{T}\right),$$

where $\underline{s}_i = (s_{i,1}, s_{i,2})$, $\ddot{\underline{s}}_i = (s_{i,1}/S_1, s_{i,2}/S_2), \ddot{t}_i = t_i/T, i = 1, 2$ for $N \le t_1, t_2 \le T - N$. In addition, assume that

$$\sum_{\kappa \in \mathbb{Z}} \left|f_{\underline{u}_1,\underline{u}_2,\tau_1,\tau_2}^{\kappa}\big(\omega_{l_1}^M, \omega_{l_2}^M\big)\right|^2 < \infty$$

and

$$\lim_{R\to\infty} R^{-1/2} \sum_{\kappa=-R}^{R} \left| f^{\kappa}_{\underline{u}_1,\underline{u}_2,\tau_1,\tau_2}\big(\omega^M_{l_1}, \omega^M_{l_2}\big) \right| = 0$$

for $\omega^M_{l_i} = \frac{2\pi l_i}{M}$, $l_i = -M, \ldots, M-1$, $i = 1, 2$.

Notice that the first part of the condition (LGR) is a generalization of the condition (L) for replicates in the considered Gaussian case. Since the replicates are not necessarily independent, the replicate-κ-shifted rescaled spatiotemporal Loève spectrum f^{κ} is not necessarily null, and consequently this fact is reflected in the additional superscript κ.

If the condition (LGR) is satisfied, then the condition (LR) is also satisfied with

$$\begin{aligned} f^{\kappa}_{\boldsymbol{u},\boldsymbol{t}}(\boldsymbol{\omega}) = {} & f^{\kappa}_{\underline{u}_1,\underline{u}_3,\tau_1,\tau_3}(\omega_1,\omega_3) f^{\kappa}_{\underline{u}_2,\underline{u}_4,\tau_2,\tau_4}(-\omega_2,-\omega_4) \\ & + f^{\kappa}_{\underline{u}_1,\underline{u}_4,\tau_1,\tau_4}(\omega_1,-\omega_4) f^{\kappa}_{\underline{u}_2,\underline{u}_3,\tau_2,\tau_3}(-\omega_2,\omega_3). \end{aligned} \tag{24}$$

Theorem 4.1. *Assume that conditions (GR), (SR) and (LGR) are fulfilled. Then the conclusions of Theorem 3.1 and of Theorem 3.2 hold.*

5 Real data application

We illustrate the application of our method on a dataset derived from an experiment in neuropsychology. It aims at improving our understanding of the brain mechanisms involved in Visual Working Memory performance. After a brief description of the scientific context and data, we demonstrate the usage of our methodology by providing a visualization of the estimated spatiotemporal dual-frequency coherence and an estimation of the dual-frequency functional connectivity networks.

5.1 Scientific context

Working Memory (WM) is an essential cognitive resource because it is strongly correlated with general cognitive abilities. Its function is to maintain access to relevant information during a brief time-span, which enables a person to perform activities such as navigation, communication, problem solving... Over the past 20 years there has been an explosion of more specific research on Visual Working Memory (VWM). Following Luck and Vogel [2013], Visual Working Memory is an "active maintenance of visual information to serve the needs of ongoing tasks". There are key issues at stake in describing and identifying sources of VWM limitation and variability, particularly from the perspective of brain connectivity [Fougnie et al., 2012]. Brain connectivity describes how localized activity can be statistically

dependent from one part of the brain to another. In the neuroscience community this is referred to as **functional connectivity** [Friston, 2011].
In our data example, the study of these brain mechanisms is based on the analysis of EEG signals. In brief, electrical currents generated in the brain by ensembles of neurons firing in a synchronized manner propagate through the cerebral cortex to the scalp, where they are recorded by spatially localized EEG electrodes. These electrodes measure electric potentials over time, which represent the oscillations of the brain waves. Hence, the study of functional connectivity can be addressed using coherence analysis. It has already been proved useful in order to reveal interesting facts about Working Memory [Sauseng et al., 2005]. A challenging aspect is that these dynamic functional connections may involve brain waves oscillatory components of different frequencies [Gorrostieta et al., 2012, Pascual-Marqui et al., 2016]. In other terms, bursts of high frequencies in some area of the brain could occur preferentially during specific phases of low frequency activity in other areas.
It is worth noticing that electrical currents at the scalp surface are spatiotemporal phenomenon sampled at the specific localization of the electrodes. We showed that our method is an appropriate tool for modeling such a phenomenon because it consistently estimates the corresponding spatio-spectral characteristics.
In fact, neuroscientists are interested in studying certain specific frequency bands that relate to different brain states and that can be interpreted in a meaningful way. More specifically, in the sequel, we consider the so-called theta, alpha and beta frequency bands ($[4, 8]$-Hz, $[8, 12]$-Hz and $[12, 20]$-Hz, respectively) denoted as Ω_θ, Ω_α and Ω_β.

5.2 Experiment and data analysis pipeline

Our real data comes from an experiment that consists of the following consecutive steps (an illustration is provided in Section 2 of the companion document Aston et al. [2022]):

- Memory set
  - Memorize: the subject is placed in front of a computer screen. An arrow appears on the screen and the subject has 2 seconds to memorize its orientation and color.
  - Retain: a blank screen appears for 0.3 seconds, then, for the next 0.1 seconds, multiple arrows appear to knock out the immediate memory. Finally, a blank screen appears again for 0.9 seconds.
- Memory test: using a joystick, the subject has 1.7 seconds to reproduce the orientation and the color of the arrow.

Notice that the subject answers about the color he remembers by selecting it from a color scale wrapped on a circle (see the companion document Aston et al. [2022]). Henceforth,

we compute the VWM errors for both orientation and color as angles between the truth and the subject's answers. This results as a set of two-dimensional VWM error measures denoted hereafter as $\{\mathbf{y}^{(r)} \in [0, 2\pi)^2 ; r = 1, \ldots, R\}$.
While the subject is performing these tasks, EEG traces are recorded using a Hydrocel GSN equipment with 129 electrodes that are placed on the subject's scalp at specific spatial locations. These electrodes record the electric potential (in micro-volts) over time with a sampling rate of 500 Hz. The subject performs this experiment $R = 2400$ times.
In the following, we denote the set of replicated spatially localized EEG traces as $\{\boldsymbol{X}_t^{\underline{s},r}, \underline{s} \in \mathcal{M}, r = 1, \ldots, R\}$, where $\mathcal{M}$ is the set of electrode coordinates in the two-dimensional plane.

Remark 5.1. *The EEG electrodes are spatially localized in 3d space over a template of the human head. Standard practice is to use projected coordinates on the 2d plane. All the information and code to obtain the 2d layout associated with the Hydrocel GSN can be obtained from Oostenveld et al. [2011].*

Remark 5.2. *We developed our method based on realistic modeling assumptions for such real data applications:*

- *Since we are interested in studying EEG connectivity and there is empirical evidence for correlations between oscillatory components of brain waves at different frequencies (see Pascual-Marqui et al. [2016]), we considered modeling these data as some kind of harmonizable processes.*
- *Along the experiment, EEGs corresponds to the electrical activity of sequence of different brain states, rapidly changing from one state to another. For example, the brain states related to visual information acquisition, memorization, joystick usage... Piecewise stationary models have been proved useful in such regime/state switching situation [Kumar et al., 2014, Schröder and Ombao, 2019].*
- *EEG signals represent a sample of a process that is inherently spatial, which justifies a spatial approach.*
- *The test subject repeats many times the same experiment. This experiment has a precisely timed performance of different tasks. This is taken into account by our model considering the same distribution of replicates. We additionally introduce short-term dependencies between replicates to account for fatigue and the effect of training.*
- **?***] shows that the Gaussian behavior of EEG is violated most of the time during mental tasks. Therefore, we do not assume Gaussianity in the main results.*

- *We use the assumptions of uniform Lipschitz continuity which we find to be mathematically convenient, while at the same time not violating fundamental properties of our real data.*

5.3 Statistical analysis

To illustrate the application of our method to real data, we proceed in three steps. We have replicated time series associated with two covariates: the orientation and the color errors. Since our estimators are computed on replicated observations, we need to cluster our replicates into meaningful subgroups according to these variables. All replicated time series in a given subgroup will be used to estimate the corresponding spectral quantities. Therefore, the first step of the analysis consists of unsupervised clustering of replicates according to the WVM scores. The second step consists of visualizing the data in order to comparison of the corresponding spatial time-varying dual-frequency coherence functions within each cluster, and finally the third step is to compare the dual-frequency connectivity networks.

5.3.1 Step 1: clustering with toroidal mixture

Figure 1 shows the bidimensional angular errors for all replicates. Note that both orientation and color errors are well centered around $(0, 0)$, meaning that on average the subject has an unbiased assessment of angle and color. We observe a seemingly more precise quality of memorization for colors than for orientations.
Our first step is to model the joint distribution of errors. Using the R package "BAMBI" [Chakraborty and Wong, 2019, 2018] and considering the weighted AIC criterion, our best fit is obtained using a two-component mixture of bivariate von Mises distributions. It gives a satisfactory clustering, as shown in Figure 1. The first subgroup of replicates (colored in red) can be interpreted as 'poor' memorization scores, the second subgroup (colored in blue) as 'good' memorization scores. The first subgroup contains approximately 10% of the total number of replicates.

5.3.2 Step 2: estimation of the spatial time-varying dual-frequency coherence

We can now proceed to the estimation of the spatial time-varying dual-frequency coherence functions for each cluster based on formula (16). In Figure (2) we present the estimated spatial dual-frequency coherence for frequency bands $(\Omega_\theta, \Omega_\alpha)$ in the group of poor VWM scores $\widetilde{\rho}_{\tau,\tau,\underline{u}_1,\underline{u}_2}(\Omega_\theta, \Omega_\alpha)$ at time $\tau = 1.2s$. The graph on the left shows the location of $\underline{u}_1 \in \mathcal{M}$. It is specified by the user. The graph on the right contains the output of our software, i.e. a topographic map of the spatial coherence $\left\{\widetilde{\rho}_{\tau,\tau,\underline{u}_1,\underline{u}_2}(\Omega_\theta, \Omega_\alpha), u_2 \in [0,1]^2\right\}$.

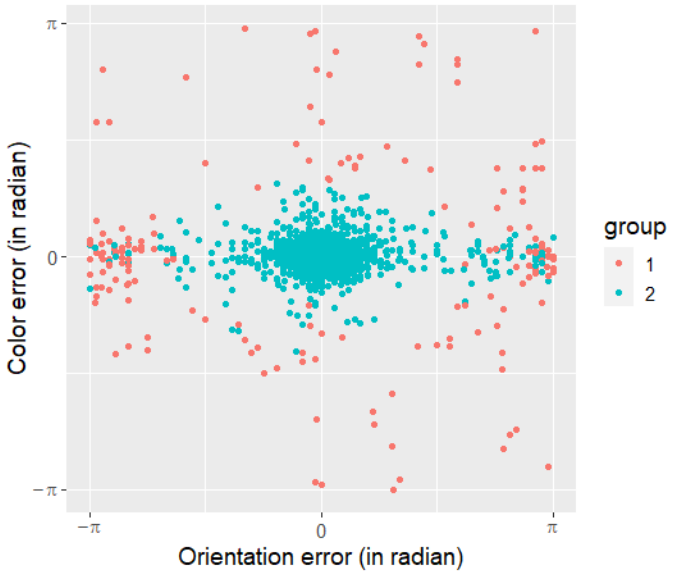

Figure 1: Angular errors associated with each replicate; x-axis: orientation error; y-axis: color error. Red and blue colors identify the subgroup resulting from unsupervised clustering.

Remark 5.3. *In this analysis and after we consider a size of the Fourier window of* 0.5 *seconds. The time window was chosen as a rule of thumb. It is an actual research question in this context to choose a proper length for the time window. It should be chosen small enough to avoid bias due to the nonstationarity and large enough to get a suitable frequency resolution.*

5.3.3 Step 3: estimation of the dual-frequency functional connectivity networks

Neuroscientists are interested in interpreting significant and sufficiently large coherence values. Hereafter, we consider that coherence values passing above 0.3 are of neurophysiological interest. We use our bootstrap approach to check whether the coherence values are above this reference value by constructing 95% left-sided bootstrap confidence intervals following Section 3. This is done for each pairs of spatial locations (here restricted to a subset of spatial locations of electrodes of interest) and for each time blocks. The block length for the CBB is taken as the integer part of the cubic root of the number of replicates. Next, we construct adjacency matrices of dual-frequency connectivity that refer to different spatial

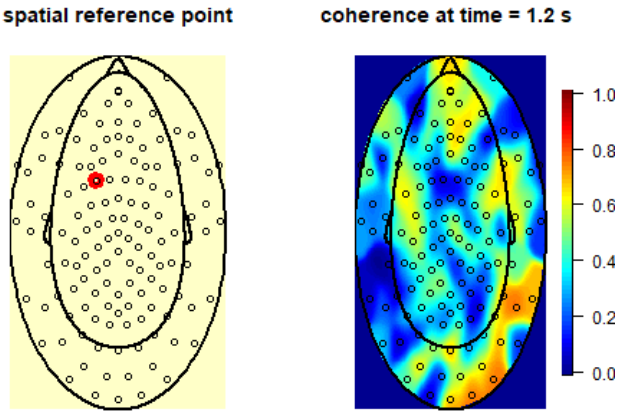

Figure 2: Estimated spatial $(\Omega_\theta, \Omega_\alpha)$ dual-frequency coherence function associated with poor VWM scores. On the left-hand side: location of $\underline{u}_1$ (user-specified); on the right-hand side: the estimated spatial coherence for all spatial locations $\underline{u}_2$.

locations at given time points. From these matrices, we construct a dynamic visualization of the network. The resulting networks of $(\Omega_\alpha, \Omega_\beta)$ dual-frequency functional connectivity at a time point of interest is shown in Figure 3. The graphs present the connectivity estimated from the set of replicates related to poor (left side) and good (right side) scores. Blue lines are drawn between spatial locations for which the lower limit of the bootstrap confidence interval for dual-frequency coherence passes over the predefined threshold value of 0.3.

More specifically, the Figure 3 reveals that brain mechanisms associated to good memorization scores exhibit significant correlation between the oscillatory components of moderate (alpha) and high (beta) frequencies within the prefrontal cortex during the memory set. Our results seem to be consistent with other known results that highlight the role of the prefrontal cortex in encoding task-relevant information in working memory tasks (Lara and Wallis [2015], Funahasi [2017]).

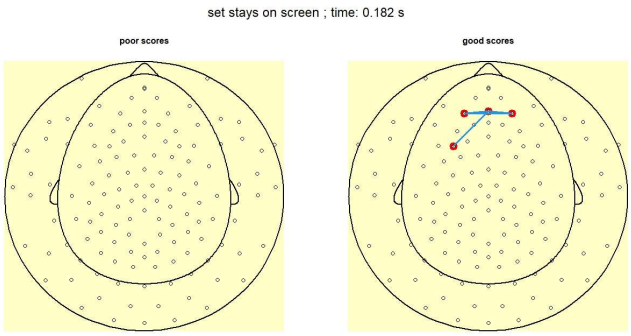

Figure 3: Statistically and neurophysiologically significant functional connections at $(\Omega_\alpha, \Omega_\beta)$ frequency bands associated with poor (left graph) and with good memorization scores (right graph).

6 Conclusions

In this paper we introduce spectral analysis for a novel model for replicated spatiotemporal processes that are locally time-harmonizable. We propose a consistent estimation procedure for the rescaled spatial time-varying Loève spectrum and the spatial time varying dual frequency coherence. We model dependency across replicated observations and we proved the consistency of the circular block bootstrap. This method allows to obtain valid confidence interval for inference. As an application example, we consider the analysis of replicated measurements of EEG signals in a neuropsychology experiment. We demonstrated the ability of our method to provide a novel way to visualize topographic maps of EEG voltage and to describe the dynamic dual-frequency functional connectivity.

Data Availability statement

The data that support the findings of this study are available on request from Prof. Denes Szucs. The data are not publicly available due to privacy and ethical restrictions.

Acknowledgements

We thank the editor and the anonymous reviewers for their comments, which helped us to improve the manuscript.

References

M. Loève. Fonctions aléatoire du second ordre. In *P. Levy's Processus Stochastiques et Mouvement Brownien*, pages 228–252. Gauthier-Villars, Paris, 1948.

P. J. Brockwell and R. A. Davis. *Time Series: Theory and Methods*. Springer Verlag, New York, 1991.

A. Napolitano. Cyclostationarity: New trends and applications. *Signal Processing*, 120: 385–408, 2016.

W.A. Gardner, A. Napolitano, and L. Paura. Cyclostationarity : half a century of research. *Signal Processing*, 86:639–697, 2006.

P. Setoodeh and S. Haykin. *Fundamentals of Cognitive Radio*. J. Wiley, Hoboken, N.J., 2017.

E. Serpedin, F. Panduru, I. Sari, and G. B. Giannakis. Bibliography on cyclostationarity. *Signal Processing*, 85:2233–2303, 2005.

H. Soedjak. Consistent estimation of the bispectral density function of a harmonizable process. *Journal of Statistical Planning and Inference*, 100(1):159–170, 2002.

C. Gorrostieta, H. Ombao, and R. von Sachs. Time-dependent dual-frequency coherence in multivariate non-stationary time series. *Journal of Time Series Analysis*, 40(1):3–22, 2019.

R. Dahlhaus. Locally stationary processes. In Tata Subba Rao, Suhasini Subba Rao, and C.R. Rao, editors, *Time Series Analysis: Methods and Applications*, volume 30, chapter 13, pages 351–413. North Holland / Elsevier, Amsterdam, 2012.

H. Ombao, X. Shao, E. Rykhlevskaia, M. Fabiani, and G. Gratton. Spatio-spectral analysis of brain signals. *Statistica Sinica*, 18:1465–1482, 2008.

J. Aston, D. Dehay, A. Dudek, J-M. Freyermuth, D. Szucs, and L. Colling. Companion document to 'spectrum inference for replicated spatial locally time-harmonizable time series'. Technical report, 2022.

P. Doukhan. *Mixing: properties and examples*. Springer series in statistics, 1994.

D. N. Politis and J. P. Romano. A circular block-resampling procedure for stationary data. In R. LePage and L. Billard, editors, *in Exploring the Limits of Bootstrap*, pages 263–270. J. Wiley, New York, 1992.

H. Künsch. The jackknife and the bootstrap for general stationary observations. *Annals of Statistics*, 17:1217–1241, 1989.

R. Liu and K. Singh. Moving block jackknife and bootstrap capture weak dependence. In R. LePage and L. Billard, editors, *In Exploring the Limits of Bootstrap*, pages 225–248. J. Wiley, Hoboken, N.J., 1992.

S. N. Lahiri. *Resampling Methods for Dependent Data*. Springer, New York, 2003.

S. J. Luck and E. K. Vogel. Visual working memory capactiy: from psychophysics and neurobiology to individual differences. *Trends in Cognitive Sciences*, 17(8):391–400, 2013.

D. Fougnie, J. Suchow, and G. Alvarez. Variability in the quality of visual working memory. *Nature communications*, 3(11):1229, 2012.

K. Friston. Functional and effective connectivity: A review. *Brain Connectivity*, 1(1):13–36, 2011.

P. Sauseng, W. Klimesch, M. Schabus, and M. Doppelmayr. Fronto-parietal eeg coherence in theta and upper alpha reflect central executive functions of working memory. *International Journal of Psychophysiology*, 57(2):97–103, 2005.

C. Gorrostieta, H. Ombao, R. Prado, S. Patel, and E. Eskandar. Exploring dependence between brain signals in a monkey during learning. *Journal of Time Series Analysis*, 33(5):771–778, 2012.

R. D. Pascual-Marqui, P. Faber, T. Kinoshita, Y. Kitaura, K. Kochi, P. Milz, K. Nishida, and M. Yoshimura. The dual frequency rv-coupling coefficient: a novel measure for quantifying cross-frequency information transactions in the brain. *arXiv:1603.05343*, 2016.

R. Oostenveld, P. Fries, E. Maris, and J-M. Schoffelen. Fieldtrip: Open source software for advanced analysis of meg, eeg, and invasive electrophysiological data. *Computational Intelligence and Neuroscience*, 2011, 2011.

T. Suneel Kumar, Vivek Kanhangad, and Ram Bilas Pachori. Classification of seizure and seizure-free eeg signals using multi-level local patterns. In *2014 19th International Conference on Digital Signal Processing*, pages 646–650, 2014. doi: 10.1109/ICDSP.2014.6900745.

A-L. Schröder and H. Ombao. Fresped: Frequency-specific change-point detection in epileptic seizure multi-channel eeg data. *Journal of the American Statistical Association*, 114(525):115–128, 2019. doi: 10.1080/01621459.2018.1476238. URL `https://doi.org/10.1080/01621459.2018.1476238`.

S. Chakraborty and S. W. K. Wong. *BAMBI: Bivariate Angular Mixture Models*, 2019. URL `https://CRAN.R-project.org/package=BAMBI`. R package version 2.1.0.

S. Chakraborty and S. W. K. Wong. Bambi: An r package for fitting bivariate angular mixture models. Technical report, 2018.

H. A. Lara and J. D. Wallis. The role of the prefrontal cortex in working memory: a mini review. *Frontiers in Neuroscience*, 18(9), 2015.

S. Funahasi. Working memory in the prefrontal cortex. *Brain Sciences*, 7(49), 2017.